Stability and stabilisation of the lattice Boltzmann method

R. A. Brownlee, A. N. Gorban and J. Levesley
Department of Mathematics, University of Leicester,
Leicester LE1 7RH UK

November 16, 2006

Abstract

The lattice Boltzmann method (LBM) is known to have stability deficiencies. For example, local blow-ups and spurious oscillations are readily observed when the method is used to model high-Reynolds fluid flow. Beginning from thermodynamic considerations, the LBM can be recognised as a discrete dynamical system generated by entropic involution and free-flight and the stability analysis is more natural. In this paper we solve the stability problem of the LBM on the basis of this thermodynamic point of view. The main instability mechanisms are identified. The simplest and most effective receipt for stabilisation adds no artificial dissipation, preserves the second-order accuracy of the method, and prescribes coupled steps: to start from a local equilibrium, then, after free-flight, perform the overrelaxation collision, and after a second free-flight step go to new local equilibrium. Two other prescriptions add some artificial dissipation locally and prevent the system from loss of positivity and local blow-up. Demonstration of the proposed stable LBMs are provided by the numerical simulation of a 1D shock tube and the unsteady 2D-flow around a square-cylinder up to Reynolds number $\mathcal{O}(10000)$.

1 Introduction

A lattice Boltzmann method (LBM) is a discrete velocity method in which a fluid is described by associating, with each velocity v_i, a single-particle distribution function $f_i = f_i(\boldsymbol{x}, t)$ which is evolved by advection and interaction on a fixed computational lattice.

The method has been proposed as a discretization of Boltzmann's kinetic transport equation:

$$\frac{\partial f_i}{\partial t} + v_i \cdot \nabla f_i = Q_i, \tag{1}$$

where the collision operator, Q_i, is subject to the fundamental mass, momentum and energy conservation laws. Dutifully, the compressible Navier–

Stokes equations are satisfied by the discrete population moments provided the studiously chosen discrete velocities have sufficient symmetry; the Mach number is sufficiently low and the long time-scale, t, is large compared to the time-scale of collisions (for an historic review see [23]). Furthermore, the collision operator can be alluringly simple, as is the case with the Bhatnager–Gross–Krook (BGK) operator [5], whereby collisions are described by a single-time relaxation to local entropy maximising equilibria f_i^* (although other choices of equilibria are often preferred [23]). Here, the relaxation time is proportional to the kinematic viscosity ν of the model.

The overrelaxation discretization of (1) (see, e.g., [4, 11, 19]) is known as LBGK and decouples viscosity from the time step, thereby suggesting that LBGK is capable of operating at arbitrarily high-Reynolds number by making the relaxation time sufficiently small. However, in this low-viscosity regime, LBGK suffers from numerical instabilities which readily manifest themselves as local blow-ups and spurious oscillations.

To analyse stability, the above historic LBM prescription is not immediately useful. However, there is another approach which arises from thermodynamic considerations. Central to this alternative prescription is the notion of an entropy maximising or *quasiequilibrium* manifold in the space of distributions and the Ehrenfests' idea of coarse-graining [14, 15]. In this new representation, the main element is the discrete (in time) dynamical system generated by entropic involution and free-flight (advection). The discrete velocities appear as approximation nodes in certain cubatures in velocity space, and if the velocities from this set are automorphisms of a lattice, the LBM in its regular space-and-time discrete form, as above, is obtained. The background knowledge necessary to discuss the LBM in this manner is presented in Sect. 2. Then, this prescription suggests several sources of numerical instabilities in the LBM and allows several receipts for stabilisation. Common to each receipt is the desire to stay uniformly *close* to the aforementioned manifold (Sect. 3).

In Sect. 5 a numerical simulation of a 1D shock tube and the unsteady 2D-flow around a square-cylinder using the present stabilised LBMs are presented. For the later problem, the simulation quantitively validates the experimentally obtained Strouhal–Reynolds relationship up to $Re = \mathcal{O}(10000)$. This extends previous LBM studies of this problem where the relationship had only been successfully validated up to $Re = \mathcal{O}(1000)$ [1, 3].

Sect. 6 contains some concluding remarks as well as practical recommendations for LBM realisations.

2 Background

In this section, we briefly introduce the thermodynamic background of our approach, and some notations. Proofs of most statements could be extracted

from [15]. Historically [23], the LBM appeared from the discretization ideas of:

1. discrete velocity set;

2. lattice space-and-time representation.

The idea of (symmetric or almost symmetric) overrelaxation was introduced to decouple viscosity from the time step [4, 11, 19, 23]. This overrelaxation was transformed into the notion of *entropic involution* [15, 21, 24], and a new understanding of the LBM was achieved. In this new representation, the main element is the discrete dynamical system generated by entropic involution and free-flight. The discrete velocity set arises as cubature approximation nodes for the hydrodynamic moments, and when these velocities are automorphisms of some lattice, the LBM in its regular space-and-time discrete form is recovered.

The lattice prescription is nice and symmetric, without any difference between space and time discretization, but it requires some effort to introduce thermodynamics and to analyse stability of systems of this kind. On the contrary, when we start from thermodynamic considerations, the entropy introduction and the stability analysis are very natural, but the cubature approximation and the space discretization requires some additional effort. Here we can find an analogy to relativistic (quantum) field theory: the Lagrangian formalism is fully covariant, but if we would like to enjoy physics of the Hamiltonian formalism, we should split space and time, and use a non-covariant representation [13].

Let us introduce *entropic involution* in earnest. The starting point is a conservative kinetic equation

$$\frac{\mathrm{d}f}{\mathrm{d}t} = J_c(f). \tag{2}$$

Here, *conservative* means that this equation preserves values of a concave functional, the entropy, $S(f)$.

The standard example is the free-flight equation

$$\frac{\partial f}{\partial t} + \boldsymbol{v} \cdot \nabla f = 0, \tag{3}$$

where $f = f(\boldsymbol{x}, \boldsymbol{v}, t)$ is a single-particle distribution function, $\boldsymbol{x}$ is the space vector, $\boldsymbol{v}$ is velocity. The choice of entropy for (3) is ambiguous; we can start from any concave functional of the form

$$S(f) = \int s(f(\boldsymbol{x}, \boldsymbol{v}, t)) f(\boldsymbol{x}, \boldsymbol{v}, t)\, \mathrm{d}\boldsymbol{x}\mathrm{d}\boldsymbol{v}$$

with concave $s(f)$. The choice by default is $s(f) = -\ln f$, which gives the classical Boltzmann–Gibbs–Shannon entropy.

In addition to the kinetic equation (2) we have a fixed linear mapping $m : f \mapsto M$ to some macroscopic variables, for example, M is the set of five hydrodynamic fields n, $n\boldsymbol{u}$ and E (density–momentum–energy),

$$M_0 = n := \int f \mathrm{d}\boldsymbol{v}, \quad M_i = nu_i := \int v_i f \mathrm{d}\boldsymbol{v}, \quad \frac{M_4}{2} = E := \frac{1}{2}\int \boldsymbol{v}^2 f \mathrm{d}\boldsymbol{v}. \tag{4}$$

Further, for each M, a quasiequilibrium (or conditional equilibrium, or generalised canonical state) f^*_M is defined as a solution of the optimisation problem

$$S(f) \to \max, \ m(f) = M. \tag{5}$$

For each f, a correspondent quasiequilibrium state $f^*_{m(f)}$ is defined. The set of all quasiequilibrium states is parameterised by M and referred to as the quasiequilibrium manifold. The projector of a point f onto the quasiequilibrium manifold is the following operator:

$$P_S : f \mapsto f^*_{m(f)}.$$

Let Θ_t be the time shift transformation for the initial conservative kinetic equation (2):

$$\Theta_t(f(0)) = f(t).$$

For the free-flight equation (3) we have

$$\Theta_t : f(\boldsymbol{x}, \boldsymbol{v}) \mapsto f(\boldsymbol{x} - \boldsymbol{v}t, \boldsymbol{v}).$$

For a given time τ, the Ehrenfests' step is a transformation of the quasiequilibrium manifold

$$\mathrm{Ehr}_\tau : f^*_M \mapsto P_S(\Theta_\tau(f^*_M)). \tag{6}$$

The motion starts on the quasiequilibrium manifold, goes time τ along the trajectory of the conservative kinetic equation (2), and then follows projection back onto the quasiequilibrium manifold. Macroscopic variables form coordinates on the quasiequilibrium manifold. In these coordinates,

$$\mathrm{Ehr}_\tau : M \mapsto m(\Theta_\tau(f^*_M)).$$

The Ehrenfests' step gives a second-order in time step τ approximation to the solution of the dissipative macroscopic equation

$$\frac{\mathrm{d}M}{\mathrm{d}t} = m(J_c(f^*_M)) + \frac{\tau}{2} m((D_f J_c(f))_{f=f^*_M} \Delta_{f^*_M}), \tag{7}$$

where $\Delta_{f^*_M}$ is the *defect of invariance* of the quasiequilibrium manifold:

$$\Delta_{f^*_M} = J_c(f^*_M) - D_M(f^*_M) m(J_c(f^*_M)), \tag{8}$$

and is the difference between the vector-field J_c and its projection on the quasiequilibrium manifold.

For the free-flight equation and hydrodynamic fields $M = M(\boldsymbol{x}, t)$ (4), the quasiequilibrium distribution is the well known local Maxwellian

$$f^*_M(\boldsymbol{v}) = n\Big(\frac{2\pi k_B T}{m}\Big)^{-3/2} \exp\Big(-\frac{m(\boldsymbol{v}-\boldsymbol{u})^2}{2k_B T}\Big),$$

and (7) is the system of compressible Navier–Stokes equations

$$\begin{aligned}
\frac{\partial n}{\partial t} &= -\sum_i \frac{\partial (n u_i)}{\partial x_i},\\
\frac{\partial (n u_j)}{\partial t} &= -\frac{1}{m}\frac{\partial P}{\partial x_j} - \sum_i \frac{\partial (n u_i u_j)}{\partial x_i}\\
&\qquad + \frac{\tau}{2}\sum_i \frac{\partial}{\partial x_i}\Big[\frac{P}{m}\Big(\frac{\partial u_j}{\partial x_i} + \frac{\partial u_i}{\partial x_j} - \frac{2\delta_{ij}}{3}\nabla\cdot\boldsymbol{u}\Big)\Big],\\
\frac{\partial E}{\partial t} &= -\frac{1}{m}\sum_i \frac{\partial (P u_i)}{\partial x_i} - \sum_i \frac{\partial (E u_i)}{\partial x_i} + \frac{\tau}{2}\frac{5k_B}{2m}\sum_i \frac{\partial}{\partial x_i}\Big(\frac{P}{m}\frac{\partial T}{\partial x_i}\Big),
\end{aligned}$$

where m is particle mass, k_{B} is Boltzmann's constant, T is kinetic temperature and $P = nk_BT$ is ideal gas pressure [18]. The dynamic viscosity is $\mu = \frac{\tau}{2}P$ (the kinematic viscosity is $\nu = \frac{\tau}{2}c_1^2$ where c_1 is the thermal velocity for one degree of freedom, $c_1^2 = k_BT/m$). For $\tau \to 0$, (7) tends to the conservative macroscopic equation

$$\frac{\mathrm{d}M}{\mathrm{d}t} = m(J_c(f^*_M)). \tag{9}$$

For hydrodynamics, this is the (compressible) Euler equations.

The step with a quasiequilibrium state *in the middle* gives a second-order in time step τ approximation to the solution of the conservative macroscopic equation (9):

$$M(0) = m(P_S(\Theta_{-\tau/2}(f^*_M))) \mapsto m(P_S(\Theta_{\tau/2}(f^*_M))) = M(\tau). \tag{10}$$

In order to decouple viscosity and time step, we can combine (6) with (10):

$$M(0) = m(P_S(\Theta_{-\vartheta/2}(f^*_M))) \mapsto m(P_S(\Theta_{\varsigma+\vartheta/2}(f^*_M))) = M(\varsigma+\vartheta) = M(\tau),$$

where $\varsigma \le \tau$ and $\vartheta = \tau - \varsigma$. The state M is a *mid-point* on the trajectory. This transformation provides a second-order in time approximation for the equation:

$$\frac{\mathrm{d}M}{\mathrm{d}t} = m(J_c(f^*_M)) + \frac{\varsigma}{2}m((D_f J_c(f))_{f=f^*_M}\Delta_{f^*_M}) \tag{11}$$

for the time step τ [15]. For the free-flight equation (3) and hydrodynamic fields (4), the system (11) is the compressible Navier–Stokes equations with dynamic viscosity $\mu = \frac{\varsigma}{2}P$ (the kinematic viscosity is $\nu = \frac{\varsigma}{2}c_1^2$).

It is worthwhile to mention that all the points $\Theta_t(f^*_M)$ belong to a manifold that is a trajectory $\mathfrak{q}$ of the quasiequilibrium manifold due to the conservative dynamics (2) (in hydrodynamic applications that is the free-flight dynamics (3)). We call this manifold the *film of non-equilibrium states* [15, 16, 17]. The defect of invariance $\Delta_{f^*_M}$ (8) is tangent to $\mathfrak{q}$ at the point f^*_M, and belongs to the intersection of this tangent space with $\ker m$. This intersection is one-dimensional. This means that the direction of $\Delta_{f^*_M}$ is selected from the tangent space to $\mathfrak{q}$ by the condition: derivative of M in this direction is zero.

A point f on the film of non-equilibrium states $\mathfrak{q}$ is naturally parameterised by (M, τ): $f = q_{M,\tau}$, where $M = m(f)$ is the value of the macroscopic variables, and $\tau = \tau(f)$ is the time shift from a quasiequilibrium state: $\Theta_{-\tau}(f)$ is a quasiequilibrium state for some (other) value of M. To the first-order in τ,

$$q_{M,\tau} = f^*_M + \tau\Delta_{f^*_M}. \tag{12}$$

The quasiequilibrium manifold divides $\mathfrak{q}$ into two parts, $\mathfrak{q} = \mathfrak{q}_- \cup \mathfrak{q}_0 \cup \mathfrak{q}_+$, where $\mathfrak{q}_- = \{q_{M,\tau} | \, \tau < 0\}$, $\mathfrak{q}_+ = \{q_{M,\tau} | \, \tau > 0\}$, and $\mathfrak{q}_0$ is the quasiequilibrium manifold: $\mathfrak{q}_0 = \{q_{M,0}\} = \{f^*_M\}$.

For each M and positive s from some interval $]0, \varsigma[$ there exist two numbers $\tau_\pm(M, s)$ ($\tau_+(M, s) > 0$, $\tau_-(M, s) < 0$) such that

$$S(q_{M,\tau_\pm(M,s)}) = S(f^*_M) - s.$$

The numbers $\tau_\pm$ coincide to the first-order: $\tau_+ = -\tau_- + o(\tau_-)$.

We define the *entropic involution* as a transformation of $\mathfrak{q}$:

$$I_S(q_{M,\tau_\pm}) = q_{M,\tau_\mp}.$$

The pair of points $f_+, f_- \in \mathfrak{q}$ connected by the involution I_S (i.e., $f_\pm = I_S(f_\mp)$) is defined (in $\mathfrak{q}$) by two conditions:

$$S(f_+) = S(f_-), \quad m(f_+) = m(f_-).$$

The values of entropy and macroscopic variables at these points coincide.

Let us choose an initial macroscopic state M_0, and suppose the initial microscopic state f_0 belongs to $\mathfrak{q}_- \cup \mathfrak{q}_+$ in a τ-small vicinity of $f^*_{M_0}$:

$$m(f_0) = M_0, \quad f_0 = q_{M,\vartheta}, \quad -\tau < \vartheta \leq 0.$$

Then the step

$$M_0 \mapsto m(I_S(\Theta_\tau(I_S(\Theta_\tau(f_0))))) \tag{13}$$

gives a second-order in time step τ approximation to the conservative macroscopic equations (9) with time step 2τ (the second application of I_S in (13) is added for symmetry and does not effect M). One shift $I_S\Theta_\tau$ guarantees first-order accuracy only [15].

For modelling the viscous motion (11) we can combine involution and projection in the following manner: for $f_0 \in \mathfrak{q}_\pm$ the point $f_1 = I_S^\beta(f_0)$, $\beta \in [1/2, 1]$, is defined in $\mathfrak{q}_\mp$ by two conditions:

$$m(f_1) = m(f_0), \quad S(f_1) - S(P_S(f_0)) = (2\beta - 1)^2 (S(f_0) - S(P_S(f_0))).$$

The point $I_S^\beta(f_0)$ is closer to the quasiequilibrium point $P_S(f_0)$ than $I_S(f_0)$. For $\beta = 1$ we get the entropic involution: $I_S^1 = I_S$, and for $\beta = 1/2$ we receive the operator $I_S^{1/2} = P_S$.

If, for $t \in [0, \tau]$, the trajectory $\Theta_t(f_0)$ intersects the quasiequilibrium manifold (i.e., $f_0 = q_{M_0,\vartheta}$ and $-\tau < \vartheta \leq 0$), then, after some initial steps, the following sequence gives a second-order in time step τ approximation of (11) with $\varsigma = (1 - \beta)\tau/\beta$, $\beta \in [1/2, 1]$:

$$M_n = m((I_S^\beta \Theta_\tau)^n f_0). \tag{14}$$

In order to prove this statement we consider a transformation of the second coordinate in $q_{M,\vartheta}$ ($-\tau < \vartheta \leq 0$): in linear approximation in ϑ and τ we have

$$(I_S^\beta \Theta_\tau) q_{M,\vartheta} = q_{M',\vartheta'},$$

where

$$\vartheta' = -(2\beta - 1)(\vartheta + \tau).$$

This transformation has a fixed point $\vartheta^* = -\tau(2\beta - 1)/(2\beta)$ and

$$(I_S^\beta \Theta_\tau)^n q_{M,\vartheta} = q_{M_n,\vartheta_n},$$

where

$$\vartheta_n = \vartheta^* + (-1)^n (2\beta - 1)^n \delta + o(\tau),$$

for some δ. This asymptotic formula is valid for the given $\beta \in [1/2, 1]$ and $\tau \to 0$, but if $1 - \beta$ is small it has no practical sense because relaxation may be too slow: $\vartheta_n \approx \vartheta^* + (-1)^n \exp(-2n(1 - \beta))\delta$, and relaxation requires $\sim 1/(1 - \beta)$ steps.

If $\vartheta_n = \vartheta^* + o(\tau)$ then the sequence M_n (14) approximates (11) with $\varsigma = \tau - 2|\vartheta^*| = (1 - \beta)\tau/\beta$ and second-order accuracy in time step τ.

As we have already mentioned, for the transfer from free-flight with entropic involution to the standard LBGK models we must:

1. transfer to a finite number of velocities with the same macroscopic equations;

2. transfer from space to a lattice, where these velocities are automorphisms;

and also,

3. transfer from dynamics and involution on $\mathfrak{q}$ to the whole space of states.

Instead of I_S^β the transformation

$$I_0^\beta : f \mapsto P_S(f) + (2\beta - 1)(P_S(f) - f) \tag{15}$$

is used. If, for a given f_0, the sequence (14) gives a second-order in time step τ approximation of (11), then the sequence

$$M_n = m((I_0^\beta \Theta_\tau)^n f_0) \tag{16}$$

also gives a second-order approximation to the same equation.

Entropic LBGK (ELBM) methods [7, 15, 21, 24] differ only in the definition of (15): for $\beta = 1$ it should conserve the entropy, and in general has the following form:

$$I_E^\beta(f) = (1 - \beta)f + \beta\tilde{f}, \tag{17}$$

with $\tilde{f} = (1 - \alpha)f + \alpha P_S(f)$. The number $\alpha = \alpha(f)$ is chosen so that the constant entropy condition is satisfied: $S(f) = S(\tilde{f})$. For LBGK (15), $\alpha = 2$.

Of course, computation of I_0^β is much easier than that of I_S^β or I_E^β: it is not necessary to follow exactly the manifold $\mathfrak{q}$ and to solve the nonlinear constant entropy condition equation. For an appropriate initial condition from $\mathfrak{q}$ (not sufficiently close to $\mathfrak{q}_0$), two steps of ELBM with I_0^β gives the same second-order accuracy as (14). But a long chain of such steps can lead far from the quasiequilibrium manifold and even from $\mathfrak{q}$. Here, we see stability problems arising.

3 Stability and receipts for stabilisation

First of all, if f is far from the quasiequilibrium, the state $I_0^\beta(f)$ may be non-physical. The positivity conditions (positivity of probabilities or populations) may be violated. For multi-dimensional and infinite-dimensional problems it is necessary to specify what one means by *far*. In the previous section, f is the whole state which includes the states of all sites of the lattice. All the inversion operators with classical entropies (ones that do not depend on gradients) are defined for lattice sites independently. Violation of positivity at one site makes the whole state non-physical. Hence, we should use here the ℓ_∞-norm: close states are close uniformly, at all sites.

There is a simple receipt for positivity preservation: to substitute non-positive $I_0^\beta(f)$ by the closest non-negative state that belongs to the straight line

$$\left\{\lambda f + (1 - \lambda)P_S(f) \middle| \, \lambda \in \mathbb{R}\right\}$$

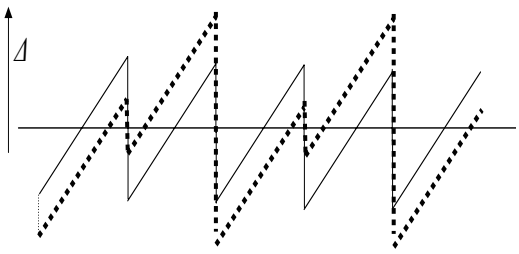

Figure 1: Neutral stability and one-step oscillations in a sequence of reflections. Bold dotted line – a perturbed motion, Δ – direction of neutral stability.

defined by the two points, f and correspondent quasiequilibrium. Let us call this receipt the *positivity rule*. It has been demonstrated [8] (also, independently, in [25]) that the classic LBGK model with the positivity rule provides the same results (in the sense of stability and absence/presence of spurious oscillations) as the entropic LBGK models. This receipt preserves positivity of populations and probabilities, but can affect accuracy of approximation: to avoid the change of accuracy order, the number of sites with this step should be of the order $\mathcal{O}(Nh/L)$ where N is the total number of sites, h is the step of the space discretization and L is the macroscopic characteristic length.

The second problem is non-linearity: for accuracy estimates we always use the assumption that f is sufficiently close to quasiequilibrium. Far from the quasiequilibrium manifold these estimates do not work because of nonlinearity (first of all, the quasiequilibrium distribution, f^*_M, depends nonlinearly on M and hence the projection operator, P_S, is nonlinear). Again we need to keep the states not far from the quasiequilibrium manifold.

The third problem is a directional instability that can affect accuracy: the vector $f - P_S(f)$ can deviate far from the tangent to $\mathfrak{q}$. Hence, we should not only keep f close to the quasiequilibrium, but also guarantee smallness of the angle between the direction $f - P_S(f)$ and tangent space to $\mathfrak{q}$.

One could rely on the stability of this direction, but we fail to prove this in any general case. The directional instability changes the structure of dissipation terms: the accuracy decreases to the first-order in τ and significant fluctuations of the Prandtl number and viscosity, etc may occur. This carries a danger even without blow-ups; one could conceivably be relying on non-reliable computational results.

Furthermore, there exists a neutral stability of all described approximations that causes one-step oscillations: a small shift of f in the direction of $\Delta_{f^*_M}$ does not relax back for $\beta = 1$, and its relaxation is slow for $\beta \sim 1$ (for small viscosity). This effect is demonstrated for a chain of mirror reflections in Fig. 1.

Three prescriptions allow us to improve the situation:

1. Positivity rule.
   The technical advise is to use this rule in all discrete kinetic models. This rule guarantees positivity of populations and probabilities, and elementary post-processing allows one to estimate how these steps affect the whole picture. Tests prove that this rule is as effective as entropic methods, and they are much simpler for realisation (see, [8] and Sect. 5).

For the stabilisation of LBMs, the entropic version of (17) was proposed and is used. This approach somehow improves stability, indeed, but cannot erase spurious oscillation and large local deviation from quasiequilibrium [6, 8, 9]. The H-theorem implies stability of equilibrium in the entropic norm (that is, a weighted ℓ_2-norm, a weighted sum of squared point evaluations) for isolated systems. For non-isolated systems (e.g., the shock tube, systems with external flows, etc.) the H-theorem (positivity of entropy production) does not guarantee stability in any norm, but can be used to establish certain estimates of boundedness with respect to the entropic norm. However, to suppress local blow-ups we need estimates in ℓ_∞-norm, and to suppress high-frequency oscillations we need boundedness in the Sobolev norm that depends on derivatives.

2. Ehrenfests' regularisation.
   In order to keep the current state uniformly close to the quasiequilibrium manifold we monitor local deviation of f from the correspondent quasiequilibrium, and when this deviation is large perform local Ehrenfests' steps [18], [1]
   $$f_j \mapsto f_j^*, \tag{18}$$
   where j is the number of the site, f_j is the state at this site, and f_j^* is the correspondent local quasiequilibrium (we assume that the entropy is the sum of nodal values, and the problem of quasiequilibrium (5) is fully split into local problems at the sites).

In order to preserve the second-order of accuracy, it is worthwhile performing Ehrenfests' steps at only a small number of sites (the number of sites should be $\mathcal{O}(Nh/L)$, where N is the total number of sites, L is the macroscopic characteristic length and h is the lattice step). If only k sites are required then this constitutes a computational cost of $\mathcal{O}(kN)$. Numerical experiments show (see, e.g., [8, 9] and Sect. 5) that even a small number of such steps drastically improves stability.

[1] In our paper [9] we used another definition that follows the Euler discretization of the BGK equation, but, for small viscosity this is essentially the same

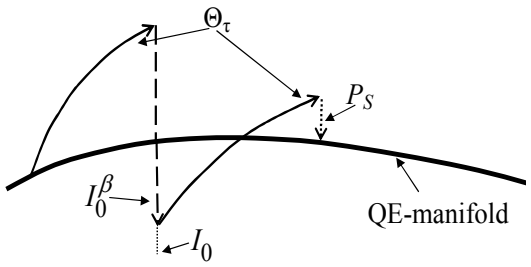

Figure 2: The scheme of coupled steps (19).

3. Coupled steps with quasiequilibrium ends.
   Let us take f_M^* as the initial state with given M, then evolve the state by Θ_τ, apply LBGK reflection I_0^β, again evolve by Θ_τ, and finally project by P_S onto quasiequilibrium manifold:

$$M \mapsto m(P_S(\Theta_\tau(I_0^\beta(\Theta_\tau(f_M^*))))) \tag{19}$$

   The analysis of entropy production easily shows that this step (Fig. 2) gives a second-order in time τ approximation to the shift in time 2τ for (11) with $\varsigma = 2(1-\beta)\tau$, $\beta \in [1/2, 1]$. The stabilisation (restart exactly from a quasiequilibrium point) introduces additional dissipation of order τ^2, and the perturbation of accuracy is of order τ^3. Hence, the method has the second-order accuracy.

It is necessary to stress that the viscosity coefficient is proportional to ς and significantly depends on the chain construction: for the sequence (14) we have $\varsigma = (1-\beta)\tau/\beta$, and for the sequence of steps (19) $\varsigma = 2(1-\beta)\tau$ (the procedure for calculating this viscosity coefficient is contained in Sect. 4). For small $1-\beta$ the later gives around two times larger viscosity (and for realisation of the same viscosity we must take this in to account).

4 Viscosity computation

In this section, we demonstrate how to compute viscosity for any construction of steps on the base of (7) and the representation (12). We compute the entropy production and compare it to the entropy production in Ehrenfests' steps.

First of all, for any f, the distribution $P_S(f) = f^*_{m(f)}$ is the entropy maximiser for the given macroscopic variables $M = m(f)$. Hence, by Taylor expansion,

$$S(f) = S(P_S(f)) + \frac{1}{2}\langle f - P_S(f), f - P_S(f)\rangle_{P_S(f)} + o(\|f - P_S(f)\|^2),$$

where $\langle \cdot, \cdot \rangle_g$ is the entropic inner-product, i.e., the negative of the bilinear form of the second differential of entropy: $\langle \varphi, \psi \rangle_g := -(D_f^2 S(f))_{f=g}(\varphi, \psi)$.

In particular, using (12), we have

$$S(q_{M,\tau}) = S(f_M^*) + \frac{\tau^2}{2} \langle \Delta_{f_M^*}, \Delta_{f_M^*} \rangle_{f_M^*} + o(\tau^2).$$

For the operation I_0^β (15) we have

$$S(I_0^\beta f) = S(P_S(f)) + \frac{(2\beta - 1)^2}{2} \langle f - P_S(f), f - P_S(f) \rangle_{P_S(f)} + o(\|f - P_S(f)\|^2).$$

In particular,

$$S(I_0^\beta q_{M,\tau}) = S(f_M^*) + \frac{\tau^2 (2\beta - 1)^2}{2} \langle \Delta_{f_M^*}, \Delta_{f_M^*} \rangle_{f_M^*} + o(\tau^2),$$

and for the correspondent entropy gain ΔS_1 we have

$$\Delta S_1 = 2\tau^2 \beta (1 - \beta) \langle \Delta_{f_M^*}, \Delta_{f_M^*} \rangle_{f_M^*} + o(\tau^2).$$

Entropy production is the ratio of entropy gain to time. For the Ehrenfests' step (6) in time τ the entropy gain $\Delta S_{\mathrm{Ehr},\tau}$ is

$$\Delta S_{\mathrm{Ehr},\tau} = \frac{\tau^2}{2} \langle \Delta_{f_M^*}, \Delta_{f_M^*} \rangle_{f_M^*} + o(\tau^2),$$

with entropy production $\sigma_{\mathrm{Ehr},\tau}$ given by the expression

$$\sigma_{\mathrm{Ehr},\tau} = \frac{\Delta S_{\mathrm{Ehr},\tau}}{\tau} = \frac{\tau}{2} \langle \Delta_{f_M^*}, \Delta_{f_M^*} \rangle_{f_M^*} + o(\tau). \tag{20}$$

Now, for a coupled step (19) (see Fig. 2)

$$f_M^* \mapsto P_S(\Theta_\tau(I_0^\beta(\Theta_\tau(f_M^*)))),$$

the free-flight does not change entropy and the entropy gain is

$$\Delta S = \Delta S_1 + \Delta S_2,$$

with $\Delta S_2 = \Delta S_{\mathrm{Ehr},2(1-\beta)\tau}$. Thus,

$$\begin{aligned} \Delta S &= 2\tau^2 \beta (1 - \beta) \langle \Delta_{f_M^*}, \Delta_{f_M^*} \rangle_{f_M^*} + 2\tau^2 (1 - \beta)^2 \langle \Delta_{f_M^*}, \Delta_{f_M^*} \rangle_{f_M^*} + o(\tau^2) \\ &= 2\tau^2 (1 - \beta) \langle \Delta_{f_M^*}, \Delta_{f_M^*} \rangle_{f_M^*} + o(\tau^2). \end{aligned}$$

The corresponding entropy production is

$$\sigma = \frac{\Delta S}{\tau} = \tau (1 - \beta) \langle \Delta_{f_M^*}, \Delta_{f_M^*} \rangle_{f_M^*} + o(\tau). \tag{21}$$

After comparison of the two entropy production formulas (20) and (21) we can immediately conclude that the coupled step (19) gives a second-order in time approximation of (11) with $\varsigma = 2(1 - \beta)\tau$. For any other variants of step construction the method of viscosity computation is the same: we estimate the entropy gain up to the second-order, and find the correspondent value of ς.

5 Numerical experiment

To conclude this paper we report two numerical experiments conducted to demonstrate the performance of the proposed LBM stabilisation receipts from Sect. 3. The first test is a 1D shock tube and we are interested in comparing the Ehrenfests' regularisation (18), the coupled step (19) with LBGK (15) and ELBM (17).

The second test is the 2D unsteady flow around a square-cylinder. The unsteady flow around a square-cylinder has been widely experimentally investigated in the literature (see, e.g., [12, 22, 26]). We demonstrate that LBGK (15), with the Ehrenfests' regularisation (18), is capable of quantitively capturing the Strouhal–Reynolds relationship. The relationship is verified up to $Re = 20000$ and compares well with Okajima's experimental data [22].

As we are advised in Sect. 3, in all of the experiments, we implement the positivity rule.

5.1 Shock tube

The 1D shock tube for a compressible isothermal fluid is a standard benchmark test for hydrodynamic codes. We will fix the kinematic viscosity of the fluid at $\nu = 10^{-9}$. Our computational domain will be the interval $[0, 1]$ and we discretize this interval with 801 uniformly spaced lattice sites. We choose the initial density ratio as 1:2 so that for $x \leq 400$ we set $n = 1.0$ else we set $n = 0.5$.

In all of our simulations we use a lattice with spacing $h = 1$, time step $\tau = 1$ and a discrete velocity set $\{v_1, v_2, v_3\} := \{0, -1, 1\}$ so that the model consists of static, left- and right-moving populations only. The governing equations for LBGK are then

$$f_i(x + v_i, t + 1) = f_i^*(x, t) + (2\beta - 1)(f_i^*(x, t) - f_i(x, t)), \qquad (22)$$

where the subscript i denotes population (not lattice site number) and f_1, f_2 and f_3 denote the static, left- and right-moving populations, respectively. The entropy is $S = -H$, with

$$H = f_1 \log(f_1/4) + f_2 \log(f_2) + f_3 \log(f_3),$$

(see, e.g., [20]) and, for this entropy, the local quasiequilibrium state f^* is available explicitly:

$$\begin{aligned} f_1^* &= \frac{2n}{3}\big(2 - \sqrt{1 + 3u^2}\big), \\ f_2^* &= \frac{n}{6}\big((3u - 1) + 2\sqrt{1 + 3u^2}\big), \\ f_3^* &= -\frac{n}{6}\big((3u + 1) - 2\sqrt{1 + 3u^2}\big), \end{aligned}$$

where

$$n := \sum_i f_i, \quad u := \frac{1}{n} \sum_i v_i f_i.$$

For contrast we are interested in comparison with ELBM (17):

$$f_i(x + v_i, t + 1) = (1 - \beta) f_i^*(x, t) + \beta \tilde{f}_i(x, t), \tag{23}$$

with $\tilde{f} = (1 - \alpha) f + \alpha f^*$. As previously mentioned, the parameter, α, is chosen to satisfy a constant entropy condition. This involves finding the nontrivial root of the equation

$$S((1 - \alpha) f + \alpha f^*) = S(f). \tag{24}$$

Inaccuracy in the solution of this equation can introduce artificial viscosity. To solve (24) numerically we employ a robust routine based on bisection. The root is solved to an accuracy of 10^{-15} and we always ensure that the returned value of α does not lead to a numerical entropy decrease. We stipulate that if, at some site, no nontrivial root of (24) exists we will employ the positivity rule instead.

For the realisation of the Ehrenfests' regularisation of LBGK, which is intended to keep states uniformly close to the quasiequilibrium manifold, we should monitor non-equilibrium entropy ΔS at every lattice site:

$$\Delta S := S(f^*) - S(f),$$

throughout the simulation. If a pre-specified threshold value δ is exceeded, then an Ehrenfests' step is taken at the corresponding site. Now, the governing equations become:

$$f_i(x + v_i, t + 1) = \begin{cases} f_i^*(x, t) + (2\beta - 1)(f_i^*(x, t) - f_i(x, t)), & \Delta S \leq \delta, \\ f_i^*(x, t), & \text{otherwise.} \end{cases} \tag{25}$$

Furthermore, so that the Ehrenfests' steps are not allowed to degrade the accuracy of LBGK it is pertinent to select the k sites with highest $\Delta S > \delta$. The a posteriori estimates of added dissipation could easily be performed by analysis of entropy production in Ehrenfests' steps.

The governing equations for the coupled step regularisation of LBGK alternates between classic LBGK and Ehrenfests' steps:

$$f_i(x + v_i, t + 1) = \begin{cases} f_i^*(x, t) + (2\beta - 1)(f_i^*(x, t) - f_i(x, t)), & N_{\text{step}} \text{ even}, \\ f_i^*(x, t), & N_{\text{step}} \text{ odd}, \end{cases} \tag{26}$$

where N_{step} is the cumulative total number of time steps taken in the simulation. Of course, one is at liberty to combine the coupled step (26) with

the Ehrenfests' regularisation (25) to create another method, and we will do this as well.

In accordance with the closing remark of Sect. 3, as the kinematic viscosity of the model fluid is fixed at $\nu = 10^{-9}$ we should take $\beta = 1/(2\nu + 1) \approx 1 - 2\nu$ for LBGK, ELBM and the Ehrenfests' regularisation. Whereas, for the coupled step regularisation, we should take $\beta = 1 - \nu$.

We observe that the proposed stabilisation receipts (25) and (26) are capable of subduing spurious post-shock oscillations whereas LBGK and ELBM fail in this respect (Fig. 3). The coupled step simulation (Fig. 3e) is strikingly impressive as the scheme introduces zero artificial dissipation. Furthermore, the small post-shock deviation in Fig. 3e (we believe this phenomenon is unavoidable without adding dissipation) can be eradicated using Ehrenfests' steps (Fig. 3f and Fig. 3g).

In the example, we have considered fixed tolerances of $(k, \delta) = (4, 10^{-3})$ and $(k, \delta) = (4, 10^{-4})$ only. We reiterate that it is important for Ehrenfests' steps to be employed at only a small share of sites. To illustrate, in Fig. 4 we have allowed k to be unbounded and let δ vary. As δ decreases, the number of Ehrenfests' steps quickly begins to grow (as shown in the accompanying histograms) and excessive and unnecessary smoothing is observed on the shock and rarefaction wave. The second-order accuracy of LBGK is corrupted. In Fig. 5, we have kept δ fixed at $\delta = 10^{-4}$ and instead let k vary. We observe that even small values of k (e.g., $k = 1$) dramatically improves the stability of LBGK.

5.2 Flow around a square-cylinder

Our second test is the 2D unsteady flow around a square-cylinder. The realisation of LBGK that we use will employ a uniform 9-speed square lattice with discrete velocities

$$v_i = \begin{cases} 0, & i = 0, \\ \left(\cos\Big((i-1)\frac{\pi}{2}\Big), \sin\Big((i-1)\frac{\pi}{2}\Big)\right), & i = 1, 2, 3, 4, \\ \sqrt{2}\left(\cos\Big((i-5)\frac{\pi}{2} + \frac{\pi}{4}\Big), \sin\Big((i-5)\frac{\pi}{2} + \frac{\pi}{4}\Big)\right), & i = 5, 6, 7, 8. \end{cases}$$

The numbering f_0, $f_1, \ldots, f_8$ are for the static, east-, north-, west-, south-, northeast-, northwest-, southwest- and southeast-moving populations, respectively. As usual, the quasiequilibrium state, f^*, can be uniquely determined by maximising an entropy functional

$$S(f) = -\sum_i f_i \log\Big(\frac{f_i}{W_i}\Big),$$

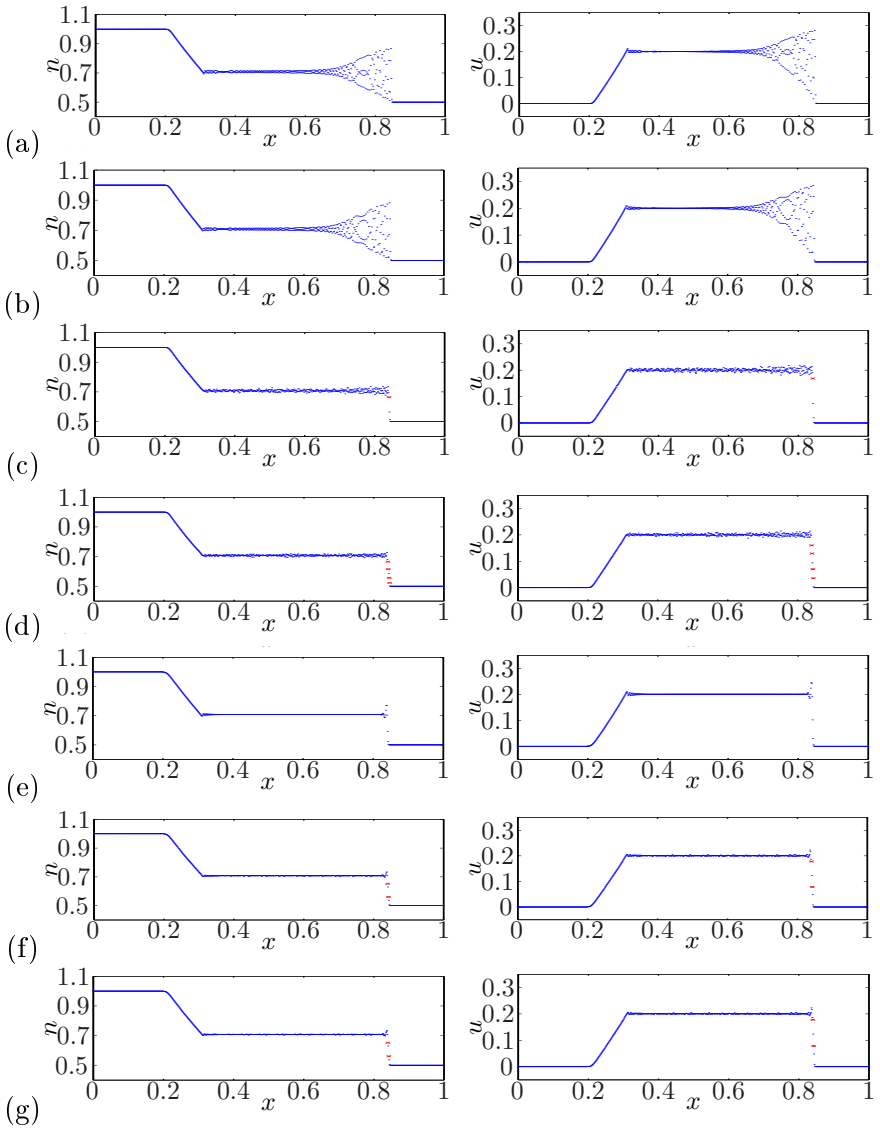

Figure 3: Density and velocity profile of the 1:2 isothermal shock tube simulation after 400 time steps using (a) ELBM (23); (b) LBGK (22); (c) Ehrenfests' regularisation (25) with $(k, \delta) = (4, 10^{-3})$; (d) Ehrenfests' regularisation (25) with $(k, \delta) = (4, 10^{-4})$; (e) coupled step regularisation (26); (f) coupled step combined with Ehrenfests' regularisation with $(k, \delta) = (4, 10^{-3})$; (g) coupled step combined with Ehrenfests' regularisation with $(k, \delta) = (4, 10^{-4})$. In this example, no negative population are produced by any of the methods so the positivity rule is redundant. For ELBM in this example, (24) always has a nontrivial root. Sites where Ehrenfests' steps are employed are indicated by crosses.

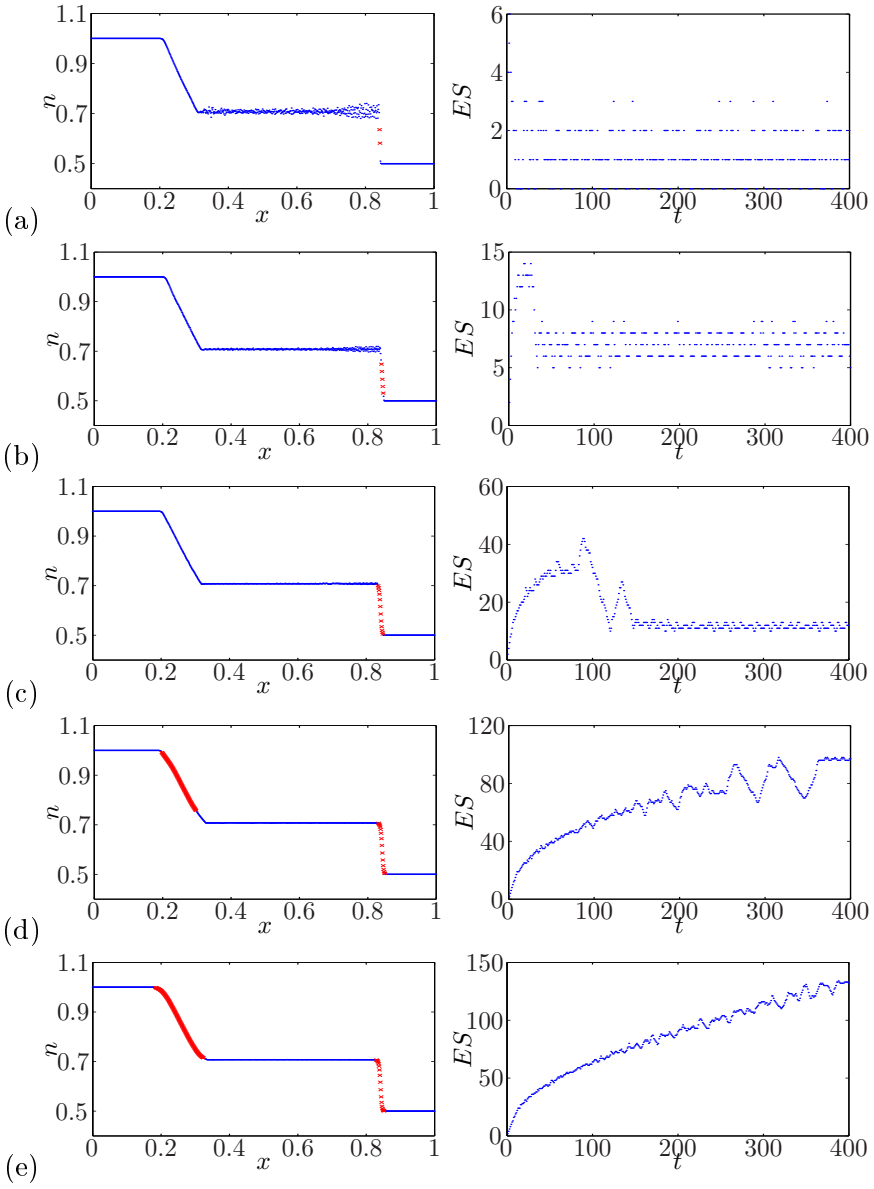

Figure 4: LBGK (22) regularised with Ehrenfests' steps (25). Density profile of the 1:2 isothermal shock tube simulation and Ehrenfests' steps histogram after 400 time steps using the tolerances (a) $(k, \delta) = (\infty, 10^{-3})$; (b) $(k, \delta) = (\infty, 10^{-4})$; (c) $(k, \delta) = (\infty, 10^{-5})$; (d) $(k, \delta) = (\infty, 10^{-6})$; (e) $(k, \delta) = (\infty, 10^{-7})$. Sites where Ehrenfests' steps are employed are indicated by crosses.

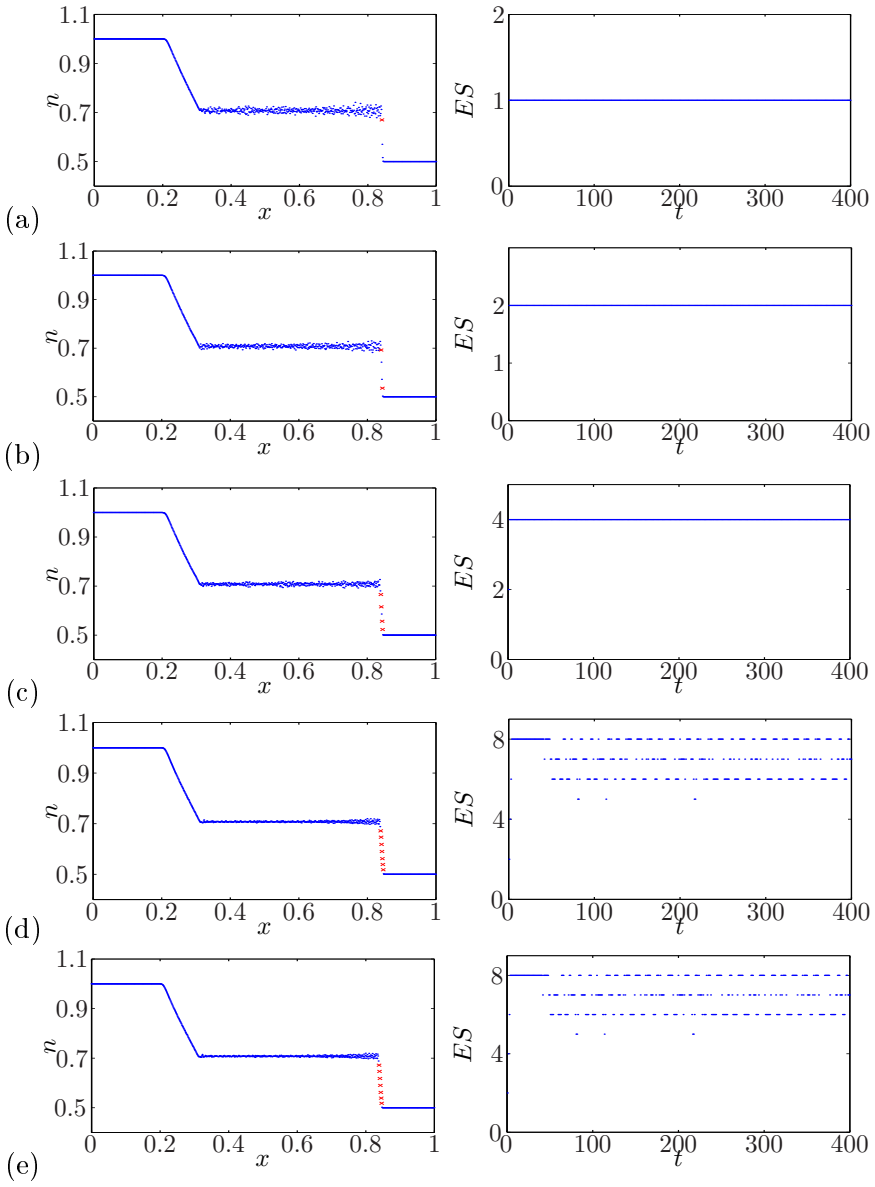

Figure 5: LBGK (22) regularised with Ehrenfests' steps (25). Density profile of the 1:2 isothermal shock tube simulation and Ehrenfests' steps histogram after 400 time steps using the tolerances (a) $(k, \delta) = (1, 10^{-4})$; (b) $(k, \delta) = (2, 10^{-4})$; (c) $(k, \delta) = (4, 10^{-4})$; (d) $(k, \delta) = (8, 10^{-4})$; (e) $(k, \delta) = (16, 10^{-4})$. Sites where Ehrenfests' steps are employed are indicated by crosses.

subject to the constraints of conservation of mass and momentum:

$$f_i^* = nW_i \prod_{j=1}^{2} \left(2 - \sqrt{1+3u_j^2}\right) \left(\frac{2u_j + \sqrt{1+3u_j^2}}{1-u_j}\right)^{v_{i,j}} \tag{27}$$

Here, the *lattice weights,* W_i, are given lattice-specific constants: $W_0 = 4/9$, $W_{1,2,3,4} = 1/9$ and $W_{5,6,7,8} = 1/36$. The macroscopic variables are given by the expressions

$$n := \sum_i f_i, \quad (u_1, u_2) := \frac{1}{n} \sum_i v_i f_i.$$

The computational set up for the flow is as follows. A square-cylinder of side length L, initially at rest, is emersed in a constant flow in a rectangular channel of length $30L$ and height $25L$. The cylinder is place on the centre line in the y-direction resulting in a blockage ratio of 4%. The centre of the cylinder is placed at a distance $10.5L$ from the inlet. The free-stream velocity is fixed at $(u_\infty, v_\infty) = (0.05, 0)$ (in lattice units) for all simulations.

On the north and south channel walls a free-slip boundary condition is imposed (see, e.g., [23]). At the inlet, the inward pointing velocities are replaced with their quasiequilibrium values corresponding to the free-stream velocity. At the outlet, the inward pointing velocities are replaced with their associated quasiequilibrium values corresponding to the velocity and density of the penultimate row of the lattice.

5.2.1 Maxwell boundary condition

The boundary condition on the cylinder that we prefer is the diffusive Maxwell boundary condition (see, e.g., [10]), which was first applied to LBMs in [2]. The essence of the condition is that populations reaching a boundary are reflected, proportional to equilibrium, such that mass-balance (in the bulk) and detail-balance are achieved. We will describe two possible realisations of the boundary condition – time-delayed and instantaneous reflection of equilibrated populations. In both instances, immediately prior to the advection of populations, only those populations pointing in to the fluid at a boundary site are updated. Boundary sites do not undergo the collisional step that the bulk of the sites are subjected to.

To illustrate, consider the situation of a wall, aligned with the lattice, moving with velocity u_{wall} and with outward pointing normal to the wall pointing in the positive y-direction (this is the situation on the north wall of the square-cylinder with $u_{\text{wall}} = 0$). The time-delayed reflection implementation of the diffusive Maxwell boundary condition at a boundary site

(x, y) on this wall consists of the update

$$\begin{aligned} f_2(x, y, t+1) &= \lambda f_2^*(u_{\text{wall}}), \\ f_5(x, y, t+1) &= \lambda f_5^*(u_{\text{wall}}), \\ f_6(x, y, t+1) &= \lambda f_6^*(u_{\text{wall}}), \end{aligned}$$

with

$$\lambda = \frac{f_4(x, y, t) + f_7(x, y, t) + f_8(x, y, t)}{f_2^*(u_{\text{wall}}) + f_5^*(u_{\text{wall}}) + f_6^*(u_{\text{wall}})}.$$

Whereas for the instantaneous reflection implementation,

$$\lambda = \frac{f_4(x, y+1, t) + f_7(x+1, y+1, t) + f_8(x-1, y+1, t)}{f_2^*(u_{\text{wall}}) + f_5^*(u_{\text{wall}}) + f_6^*(u_{\text{wall}})}.$$

Observe that, because density is a linear factor of the equilibria (27), the density of the wall is inconsequential in the boundary condition and can therefore be taken as unity for convenience.

We point out that, although both realisations agree in the continuum limit, the time-delayed implementation does not accomplish mass-balance. Therefore, instantaneous reflection is preferred and will be the implementation that we employ in the present example.

Finally, it is instructive to illustrate the situation for a boundary site (x, y) on a corner of the square-cylinder, say the north-west corner. The (instantaneous reflection) update is then

$$\begin{aligned} f_2(x, y, t+1) &= \mu f_2^*(u_{\text{wall}}), \\ f_3(x, y, t+1) &= \mu f_3^*(u_{\text{wall}}), \\ f_5(x, y, t+1) &= \mu f_5^*(u_{\text{wall}}), \\ f_6(x, y, t+1) &= \mu f_6^*(u_{\text{wall}}), \\ f_7(x, y, t+1) &= \mu f_7^*(u_{\text{wall}}), \end{aligned}$$

where

$$\begin{aligned} \mu = \big(&f_1(x-1, y, t) + f_4(x, y+1, t) + f_5(x-1, y-1, t) \\ &+ f_7(x+1, y+1, t) + f_8(x-1, y+1, t)\big) \\ &\Big/ \big(f_2^*(u_{\text{wall}}) + f_3^*(u_{\text{wall}}) + f_5^*(u_{\text{wall}}) + f_6^*(u_{\text{wall}}) + f_7^*(u_{\text{wall}})\big). \end{aligned}$$

5.2.2 Strouhal–Reynolds relationship

As a test of the Ehrenfests' regularisation (18), a series of simulations, all with characteristic length fixed at $L = 20$, were conducted over a range of Reynolds numbers

$$Re = \frac{L u_\infty}{\nu}.$$

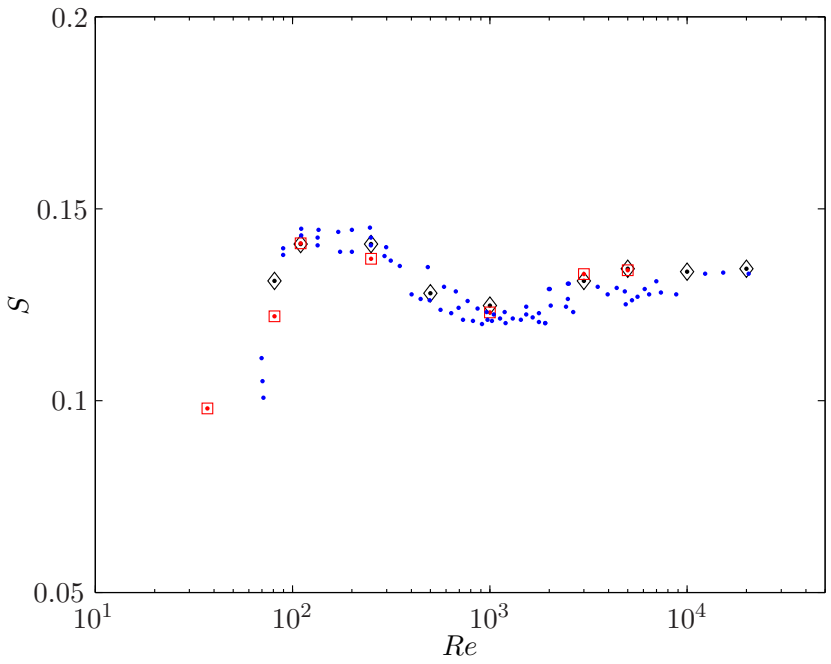

Figure 6: Variation of Strouhal number as a function of Reynolds. Dots are Okajima's experimental data [22] (the data has been digitally extracted from the original paper). Diamonds are the Ehrenfests' regularisation of LBGK and the squares are the ELBM simulation from [1].

The parameter pair (k, δ), which control the Ehrenfests' steps tolerances, are fixed at $(L/2, 10^{-3})$.

We are interested in computing the Strouhal–Reynolds relationship. The Strouhal number S is a dimensionless measure of the vortex shedding frequency in the wake of one side of the cylinder:

$$S = \frac{L f_\omega}{u_\infty},$$

where f_ω is the shedding frequency.

For our computational set up, the vortex shedding frequency is computed using the following algorithmic technique. Firstly, the x-component of velocity is recorded during the simulation over $t_{\max} = 1250L/u_\infty$ time steps. The monitoring points is positioned at coordinates $(4L, -2L)$ (assuming the origin is at the centre of the cylinder). Next, the dominant frequency is extracted from the final 25% of the signal using the discrete Fourier transform. The monitoring point is purposefully placed sufficiently downstream and away from the centre line so that only the influence of one side of the cylinder is recorded.

The computed Strouhal–Reynolds relationship using the Ehrenfests' reg-

ularisation of LBGK is shown in Fig. 6. The simulation compares well with Okajima's data from wind tunnel and water tank experiment [22]. The present simulation extends previous LBM studies of this problem [1, 3] which have been able to quantitively captured the relationship up to $Re = \mathcal{O}(1000)$. Fig. 6 also shows the ELBM simulation results from [1]. Furthermore, the computational domain was fixed for all the present computations, with the smallest value of the kinematic viscosity attained being $\nu = 5 \times 10^{-5}$ at $Re = 20000$. It is worth mentioning that, for this characteristic length, LBGK exhibits numerical divergence at around $Re = 1000$. We estimate that, for the present set up, the computational domain would require at least $\mathcal{O}(10^7)$ lattice sites for the kinematic viscosity to be large enough for LBGK to converge at $Re = 20000$. This is compared with $\mathcal{O}(10^5)$ sites for the present simulation.

6 Conclusions

We have presented the main mechanisms of observed LBM instabilities:

1. Positivity loss due to high local deviation from (quasi)equilibrium;
2. Appearance of neutral stability in some directions in the zero viscosity limit;
3. Directional instability.

We found three methods of stability preservation. Two of them, the positivity rule and the Ehrenfests' regularisation, are "salvation" (or "SOS") operations. They preserve the system from positivity loss or from the local blow-ups, but introduce artificial dissipation and it is necessary to control the number of sites where these steps are applied. In order to preserve the second-order of LBM accuracy, it is worthwhile to perform these steps on only a small number of sites; the number of sites should not be higher than $\mathcal{O}(Nh/L)$, where N is the total number of sites, L is the macroscopic characteristic length and h is the lattice step. The added dissipation could easily be estimated a posterior by summarising the entropy production of the "SOS" steps.

But most effective is the special new choice of collisions: the coupled steps (26). These steps alternate between classic LBM and Ehrenfests' steps, introduce no artificial viscosity, have the second-order accuracy, and provide directional stability as well as obliterate the effects of neutral stability. Indeed, the shock tube simulation in Fig. 3e is a compelling demonstration of the proposed scheme's capabilities. Furthermore, the coupled step introduces no additional computational cost compared to classical LBMs.

The practical recommendation is to always use the coupled steps, and to keep the positivity rule and the Ehrenfests' steps as an "SOS" in reserve

in order to make rare corrections of positivity loss and of too high local deviation from equilibrium.

Acknowledgements

The first author is grateful to Shyam Chikatamarla for providing the digitally extracted data used in Fig. 6.

This work is supported by Engineering and Physical Sciences Research Council (EPSRC) grant number GR/S95572/01.

References

[1] S. Ansumali, S. S. Chikatamarla, C. E. Frouzakis, and K. Boulouchos. Entropic lattice Boltzmann simulation of the flow past square-cylinder. *Int. J. Mod. Phys. C*, 15:435–445, 2004.

[2] S. Ansumali and I. V. Karlin. Kinetic boundary conditions in the lattice Boltzmann method. *Phys. Rev. E*, 66(2):026311, 2002.

[3] G. Baskar and V. Babu. Simulation of the unsteady flow around rectangular cylinders using the ISLB method. In *34th AIAA Fluid Dynamics Conference and Exhibit*, pages AIAA–2004–2651, 2004.

[4] R. Benzi, S. Succi, and M. Vergassola. The lattice Boltzmann-equation - theory and applications. *Physics Reports*, 222(3):145–197, 1992.

[5] P. L. Bhatnager, E. P. Gross, and M. Krook. A model for collision processes in gases. I. Small amplitude processes in charged and neutral one-component systems. *Phys. Rev.*, 94:511–525, 1954.

[6] B. M. Boghosian, P. J. Love, and J. Yepez. Entropic lattice Boltzmann model for Burgers equation. *Phil. Trans. Roy. Soc. A*, 362:1691–1702, 2004.

[7] B. M. Boghosian, J. Yepez, P. V. Coveney, and A. J. Wager. Entropic lattice Boltzmann methods. *R. Soc. Lond. Proc. Ser. A Math. Phys. Eng. Sci.*, 457(2007):717–766, 2001.

[8] R. A. Brownlee, A. N. Gorban, and J. Levesley. Stabilisation of the lattice-Boltzmann method using the Ehrenfests' coarse-graining. *cond-mat/0605359*, 2006.

[9] R. A. Brownlee, A. N. Gorban, and J. Levesley. Stabilisation of the lattice-Boltzmann method using the Ehrenfests' coarse-graining. *Phys. Rev. E*, 74:037703, 2006.

[10] C. Cercignani. *Theory and Application of the Boltzmann Equation.* Scottish Academic Press, Edinburgh, 1975.

[11] S. Chen and G. D. Doolen. Lattice boltzmann method for fluid flows. *Annu. Rev. Fluid. Mech.*, 30:329–364, 1998.

[12] R. W. Davis and E. F. Moore. A numerical study of vortex shedding from rectangles. *J. Fluid Mech.*, 116:475–506, 1982.

[13] P. A. M. Dirac. *Lectures on Quantum Mechanics.* Dover Books on Physics. Dover, Mineola, NY, 2001.

[14] P. Ehrenfest and T. Ehrenfest. *The conceptual foundations of the statistical approach in mechanics.* Dover Publications Inc., New York, 1990.

[15] A. N. Gorban. Basic types of coarse-graining. In A. N. Gorban, N. Kazantzis, I. G. Kevrekidis, H.-C. Öttinger, and C. Theodoropoulos, editors, *Model Reduction and Coarse-Graining Approaches for Multiscale Phenomena*, pages 117–176. Springer, Berlin-Heidelberg-New York, 2006. cond-mat/0602024.

[16] A. N. Gorban and I. V. Karlin. Geometry of irreversibility: The film of nonequilibrium states. Preprint IHES/P/03/57, Institut des Hautes Études Scientifiques, Bures-sur-Yvette, France, 2003. cond-mat/0308331.

[17] A. N. Gorban and I. V. Karlin. *Invariant manifolds for physical and chemical kinetics*, volume 660 of Lect. Notes Phys. Springer, Berlin-Heidelberg-New York, 2005.

[18] A. N. Gorban, I. V. Karlin, H. C. Öttinger, and L. L. Tatarinova. Ehrenfest's argument extended to a formalism of nonequilibrium thermodynamics. *Phys. Rev. E*, 62:066124, 2001.

[19] F. Higuera, S. Succi, and R. Benzi. Lattice gas – dynamics with enhanced collisions. *Europhys. Lett.*, 9:345–349, 1989.

[20] I. V. Karlin, A. Ferrante, and H. C. Öttinger. Perfect entropy functions of the lattice Boltzmann method. *Europhys. Lett.*, 47:182–188, 1999.

[21] I. V. Karlin, A. N. Gorban, S. Succi, and V. Boffi. Maximum entropy principle for lattice kinetic equations. *Rev. Lett.*, 81:6–9, 1998.

[22] A. Okajima. Strouhal numbers of rectangular cylinders. *J. Fluid Mech.*, 123:379–398, 1982.

[23] S. Succi. *The lattice Boltzmann equation for fluid dynamics and beyond.* OUP, New York, 2001.

[24] S. Succi, I. V. Karlin, and H. Chen. Role of the H theorem in lattice Boltzmann hydrodynamic simulations. *Rev. Mod. Phys.*, 74:1203–1220, 2002.

[25] F. Tosi, S. Ubertini, S. Succi, H. Chen, and I. V. Karlin. Numerical stability of entropic versus positivity-enforcing lattice Boltzmann schemes. *Math. Comput. Simulation*, 72:227–231, 2006.

[26] B. J. Vickery. Fluctuating lift and drag on a long cylinder of square cross-section in a smooth and in a turbulent stream. *J. Fluid Mech.*, 25:481–494, 1966.